Massive galaxies today

The intriguing life of massive galaxies
Proceedings IAU Symposium No. 295, 2012
D. Thomas, A. Pasquali & I. Ferreras, eds.

doi:10.1017/S174392131300481X

Dark matter in massive galaxies

Ortwin Gerhard

Max-Planck-Institut für extraterrestrische Physik,
Postfach 1312, Giessenbachstr., 85741 Garching, Germany
email: gerhard@mpe.mpg.de

Abstract. The spatial distributions of luminous and dark matter in massive early-type galaxies (ETGs) reflect the formation processes which shaped these systems. This article reviews the predictions of cosmological simulations for the dark and baryonic components of ETGs, and the observational constraints from lensing, hydrostatic X-ray gas atmospheres, and outer halo stellar dynamics.

Keywords. (cosmology:) dark matter; galaxies: elliptical and lenticular, cD; galaxies: halos; galaxies: formation; galaxies: kinematics and dynamics; X-rays: galaxies; gravitational lensing

1. Introduction

A galaxy's dark matter mass is arguably the most important parameter characterizing its evolutionary state. Massive early-type galaxies (ETGs) with virial masses of up to $\sim 10^{13}\,\mathrm{M}_\odot$ are those that have evolved furthest in the galaxy building process, with little gas left to make new stars. In the centers of ETGs the luminous matter dominates, but already at a few half-light radii (R_e) of the stellar distribution, dark matter (DM) takes over. The spatial distributions of luminous and dark matter in the inner regions of ETGs are the outcome of the formation processes by which these systems were shaped, and are thus one of the observational constraints we have on these processes, next to scaling relations, stellar population properties, and orbital structure.

The following sections review first the predictions of cosmological simulations for the structure of the dark halos and baryonic components in ETGs, and then what has been learnt about their dark matter halos from different techniques: lensing, hydrostatic hot X-ray gas atmospheres, and stellar dynamics of halo tracers.

2. Dark matter halos from cosmological simulations

2.1. *Dark matter-only simulations*

Simulations of structure formation in a Cold Dark Matter Universe have progressed greatly over several decades (see Diemand & Moore 2011, for a detailed review). For the idealized case of dark matter only, without baryons, resimulations of individual halos now reach $\mathrm{O}(10^6)$ particles per halo. The main results from these studies are:

- Mass density profiles are approximately universal, i.e., independent of halo mass and cosmological parameters aside from scalings. The best current density profile model is a 3-parameter Einasto profile (Navarro *et al.* 1996; Bullock *et al.* 2001; Diemand *et al.* 2004; Navarro *et al.* 2010).
- Halo concentrations are in the range $c = r_{\rm vir}/r_s \simeq$ 5-15 with scatter at given mass $\Delta \log c \simeq 0.2$. Early-forming halos and smaller halos have higher median concentrations (Navarro *et al.* 1996; Bullock *et al.* 2001; Macciò *et al.* 2008).
- Halo shapes are strongly flattened, prolate-triaxial. The mean $\langle c/a\rangle = 0.5 \pm 0.1$. The elongation is larger at the center. It is approximately stable at fixed radius except in

major mergers, and is mostly due to anisotropy (median $\lambda \simeq 0.04$) (Dubinski & Carlberg 1991; Jing & Suto 2002; Allgood *et al.* 2006; Hayashi *et al.* 2007).

• Bound substructures are abundant but not dominant, comprising $\sim 10\%$ of the halo mass. They have a steeply declining cumulative abundance distribution with mass, $\propto (V_{\rm max}/V_{\rm max,host})^{-3}$ or $\propto M^{-2}$ (Klypin *et al.* 1999; Gao *et al.* 2004; Springel *et al.* 2008; Diemand *et al.* 2008).

• The inner density profiles are cuspy, increasing inwards. The asymptotic inner slope is now known to be slightly shallower than -1 (Navarro *et al.* 1996; Moore *et al.* 1998; Diemand *et al.* 2004; Navarro *et al.* 2010).

2.2. *Effects of baryons; alignment*

The structure of the simulated DM halos is modified by the gravitational interaction with the baryonic component, and thus indirectly by baryonic cooling, settling, star formation and feedback. The resulting modifications of the halos include:

• Steepening of the halo density profile: adiabatic contraction through slow dissipative settling of gas into a disk (Blumenthal *et al.* 1986; Gnedin *et al.* 2004; Sellwood & McGaugh 2005).

• Flattening of the cusp by feedback and shaking (Gnedin & Zhao 2002; Mashchenko *et al.* 2008; Governato *et al.* 2010; Macciò *et al.* 2012).

• The halo becomes more spherical and evolves towards oblate at all radii but mostly in its inner parts (Kazantzidis *et al.* 2004; Bailin *et al.* 2005; Berentzen & Shlosman 2006; Abadi *et al.* 2010).

• Minor axes of the disk and inner halo ($r < 0.1 r_{\rm vir}$) align when a disk forms. The minor axis orientation of the outer halo remains unchanged. As a result, the orientations of the inner and outer halo are uncorrelated in simulations with baryons, while well-aligned in N-body-only simulations (Bailin *et al.* 2005; Bailin & Steinmetz 2005; Deason *et al.* 2011).

• The angular momenta of disk and inner halo also align, whereas the median misalignment between inner and outer halo angular momenta is $\sim$ 25-45 deg (Bett *et al.* 2010; Hahn *et al.* 2010). Because the halos rotate slowly, shape and angular momentum need not be tightly correlated. Stacking of simulated halos washes out the alignment signal for weak lensing.

2.3. *Mass structure of simulated early-type galaxies*

High-resolution models of ETGs in a cosmological setting are of particular interest for comparing with the empirical results discussed in later sections of this review. Wu *et al.* (2012) analyzed 42 galaxies with stellar masses of 2.7×10^{10}–$4.7 \times 10^{11}\,{\rm M}_\odot$ from the cosmological hydrodynamical resimulations of Oser *et al.* (2010, 2012) which include a model for cooling, supernova feedback, and star formation processes, but do not include AGN feedback. These systems contain an in-situ component made in efficient early star formation, and later grow by accretion through mostly minor mergers.

Their stellar density distributions at $z = 0$ are approximately described by Sersic profiles with realistic values of n and R_e. As measure of their mass distributions, Wu *et al.* (2012) determined circular velocity curves (CVCs) $v_c \equiv [GM(r)/r]^{1/2}$. The dark matter CVCs are essentially described by power laws outside radii greater than the softening radius ($0.9h^{-1}$ kpc for DM particles). They vary systematically in that the average slope of the dark matter CVC increases with increasing circular velocity, or mass, from approximately flat at low masses to slightly rising ($\simeq 0.3$) at high masses. When the stellar component is added in, the total CVC slope changes from slightly falling ($\simeq -0.3$) at low masses to flat at high masses (see Fig. 1a). The slopes of dark matter

CVCs and total CVCs correlate with n. Typical DM fractions in the simulated ETGs are $\sim 20\%$ at $1R_e$ and $\sim 50\%$ at $5R_e$. They increase with R_e in kpc, with n, or with mass within R_e; see Wu *et al.* (2012). These results are broadly consistent with the mass profiles determined from lensing, X-rays and dynamics, as described in the following.

3. Dark matter halos of massive elliptical galaxies from lensing and X-rays

3.1. *Halo masses and shapes from weak lensing*

Halo masses for low redshift ($z < 0.35$) galaxies are constrained best by SDSS data (for other work with smaller samples, see Brainerd *et al.* 1996; Fischer *et al.* 2000; Hoekstra *et al.* 2004, 2005; Gavazzi *et al.* 2007). The weak galaxy-galaxy lensing signal for 350,000 lenses ($z < 0.35$) from SDSS was compared to a halo model based on simulations (dn/dM, NFW density profile, satellite model) by Mandelbaum *et al.* (2006b). Satisfactory agreement was found; within this model an L^* galaxy with $M^* = 6 \times 10^{10}\,\mathrm{M}_\odot$ is hosted by a halo of mass $1.4 \times 10^{12} h^{-1}\,\mathrm{M}_\odot$. This value is similar for ETGs in high and low density regions. Results from the 2 mag deeper RCS2 survey already suggested changes with redshift (van Uitert *et al.* 2011); see also the talk by Hudson in these proceedings.

In principle, weak lensing is also the method of choice to measure the outer halo shapes: individual halos will have stronger shear signal on the projected major axis than on the projected minor axis. However, a measurement of this effect requires stacking of multiple galaxies. Thus the signal is preserved only if halos and galaxies are aligned. Simulations suggest that this is not the case and that the signal is isotropized; see §2. Lensing studies by Hoekstra *et al.* (2004); Mandelbaum *et al.* (2006a); Parker *et al.* (2007); van Uitert *et al.* (2012) have detected differing lensing anisotropy signals. These studies generally indicate triaxial halos but details are still unclear.

3.2. *Dark matter mass profiles from strong lensing*

Strong lensing (see, e.g., Treu 2010) gives an accurate measurement of the projected mass within the lens Einstein radius, R_E. For lenses at $z \sim 1$, $R_E \sim$ several R_e and is located where the DM mass dominates. In this case, the DM can be studied directly, at least in high-mass ETGs ($\sigma > 200$ km/s) which dominate the samples. For most low-z lenses, $R_E < R_e$; thus the strong lensing analysis measures the combined mass from stars and DM within R_E. Mass profiles can be determined by combining multiple systems with different R_E (Rusin & Kochanek 2005; Bolton *et al.* 2008; Grillo 2012), or by mass reconstruction methods applied to the source images (Ferreras *et al.* 2005; Leier *et al.* 2011). The overal result from these studies is that on average DM starts to dominate at $\sim$ 2-3R_e.

By combining $M(< R_E)$ with a measured central velocity dispersion or resolved dispersion profile, it is possible to constrain the average slope of the mass density profile, α. Results from the SLACS sample show that the density slopes are approximately isothermal ($\alpha = 2$) (Treu & Koopmans 2004; Koopmans *et al.* 2006; Gavazzi *et al.* 2007; Barnabè *et al.* 2009; Auger *et al.* 2010). This is equivalent to a flat CVC in spirals and has been dubbed the "bulge-halo conspiracy". Barnabè *et al.* (2009, 2011) also measure halo axis ratios with axisymmetric models, obtaining values as flattened or rounder than the axis ratios of the stellar components. Adopting a Salpeter IMF, the DM fraction inside R_E is found to increase from 25% for $\sigma = 200$ km/s, $M^* = 10^{11}\,\mathrm{M}_\odot$ to 70% for $\sigma = 350$ km/s, $M^* = 10^{12}\,\mathrm{M}_\odot$ (Treu 2010). Massive ETGs must either be more dark matter dominated in their cores, or have a heavier, non-universal IMF (Auger *et al.* 2010; Treu *et al.* 2010).

3.3. *Hydrostatic mass distributions for X-ray bright ellipticals*

X-ray observations of the hot gas in massive ETGs have long been an important and independent tracer of their DM halos (Buote & Humphrey 2012). The hot gas extends to large radii where the DM dominates, and the isotropic pressure makes the analysis much simpler than for stellar tracers. With *Chandra* and *XMM-Newton*, it is no longer a problem to measure temperature profiles. Thus the current main uncertainties are whether the gas is in approximate hydrostatic equilibrium, and how large are non-thermal contributions to the pressure which are not traced by the X-ray data, such as from relativistic particles, turbulent motions and magnetic fields.

Some of the main conclusions are as follows:

- In galaxies with X-ray luminosities $L_X < 10^{39} - 10^{40}$ erg/s (depending on the optical luminosity, often lower mass systems) the X-ray flux from the hot gas is subdominant compared to that from X-ray binaries and stars, so mass determination is unreliable (Revnivtsev *et al.* 2008; Trinchieri *et al.* 2008).
- A fraction of the more X-ray luminous systems have strongly disturbed X-ray atmospheres (Diehl & Statler 2007), so that the hydrostatic equilibrium assumption is doubtful. Ciotti & Pellegrini (2004) quantified how inflows or outflows would disturb mass measurements. Reliable mass determinations are only possible in morphologically and dynamically relaxed systems (Buote & Humphrey 2012).
- In X-ray bright and relaxed galaxies, the dark matter is clearly detected and the inferred potentials are near-isothermal, i.e., the CVC is approximately flat to large radii (Humphrey *et al.* 2006, 2012; Churazov *et al.* 2008, 2010; Nagino & Matsushita 2009). The inferred DM fraction at $2R_e$ is $\sim$ 40-80%. Das *et al.* (2010) using data from Churazov *et al.* (2010) found that the CVCs turn up at large radii, possibly due to the surrounding group DM halo, and that the typical circular velocity $v_c(R_e)$ correlates with the velocity dispersion of the sub-Mpc group environment.
- Comparing determinations of the gravitational potential or CVC for the same galaxy from X-ray and optical observations gives a way to estimate the non-thermal contributions to the total pressure. Values found are between $\sim$ 10% in quiescent galaxies like NGC 1399 to $\sim$ 30% in more disturbed systems like M87 (Churazov *et al.* 2008, 2010; Das *et al.* 2011), with large uncertainties because of possible systematic effects in both techniques.

4. Dark matter halos from dynamics

4.1. *Kinematic halo tracers*

Traditional long-slit kinematics reaches down to surface brightnesses of $\mu_V \sim 23.5$ corresponding to $R \sim 2R_e$ (e.g. Kronawitter *et al.* 2000). To determine the DM mass profile and the halo orbit distribution, alternative data are therefore needed which reach to larger radii and fainter surface brightnesses, such as

- Planetary nebulae (PNe) velocities measured from their bright [OIII] emission line (e.g. Hui *et al.* 1995; Arnaboldi *et al.* 1996; Méndez *et al.* 2001; Peng *et al.* 2004). PNe are generally good tracers of the stellar light and kinematics in ETGs (Coccato *et al.* 2009). Useful kinematic information can typically be derived to $\sim$ 5-8R_e, and up to beyond 100 kpc in some cases (Doherty *et al.* 2009), reaching $\mu_V \sim 27.5$.
- Globular cluster (GC) velocities measured from their absorption line spectra (e.g. Côté *et al.* 2001; Hwang *et al.* 2008; Schuberth *et al.* 2010; Woodley *et al.* 2010). Especially bright, central ETGs contain large GC systems reaching to very large radii. The use of GCs as mass tracers is somewhat complicated by the fact that they do not trace

the galaxy light directly, requiring simultaneous determination of their (completeness-corrected) number density profile.

- Stacked absorption line spectra from integral field units (IFU) placed at large galactocentric radii. This method has been employed using the Sauron (Weijmans *et al.* 2009) and VIRUS-P (Murphy *et al.* 2011) IFU instruments and reaches down to $\mu_V \sim 25.5$.
- Stacked absorption line spectra from off-target pixels in slitlets originally placed in the halo to measure globular cluster velocities (Proctor *et al.* 2009; Foster *et al.* 2011), reaching $\mu_V \sim 25$.

4.2. *Outer halo kinematics from planetary nebulae*

While in early work with 4m telescopes velocities could be measured only for the brightest $\sim$ 30-50 PNe in ETGs at Virgo distance (e.g. Arnaboldi *et al.* 1996, 1998), we now have $\sim$ 20 ETGs with hundreds of measured PN velocities for tracing the velocity field out to large radii, typically 5-8R_e. This is mostly thanks to slitless spectroscopy efforts at the VLT (Méndez *et al.* 2001; Teodorescu *et al.* 2005, 2011; McNeil *et al.* 2010; McNeil-Moylan *et al.* 2012) and to data from the special-purpose PN.S instrument (Douglas *et al.* 2007; Coccato *et al.* 2009; Napolitano *et al.* 2009, 2011). The kinematic properties of ETG halos derived from these PN samples include (see Coccato *et al.* 2009):

- The ratio of mean velocity $\bar{v}$ and dispersion σ in the halo correlates with that within R_e for the greater part of the sample, but some galaxies are more rotationally dominated in their halos.
- The division into slow and fast rotators defined by the kinematics within $\sim R_e$ (Emsellem *et al.* 2007), is largely preserved in the outer halos. A few galaxies have more complex profiles of the angular momentum-related λ_R parameter.
- Kinematic misalignments appear to be more frequent in the halos.
- The radial profiles of rms velocity $\bar{v}^2 + \sigma^2$ fall into two groups, the major group characterized by a slow radial decrease, and a second group with "quasi-Keplerian", steeply falling profiles, first drawn attention to by Méndez *et al.* (2001) and Romanowsky *et al.* (2003).

4.3. *Kinematic substructure*

Cosmological galaxy assembly models predict that massive galaxies grow by accreting smaller companions. During and after minor merger events, photometric and kinematic substructure would be visible in the outer halo of the host galaxy where dynamical timescales are long. This is an interesting subject (and opportunity) by itself, but is also relevant for dynamical mass determinations at large radii. One example is the nearby BCG galaxy NGC 1399, studied by McNeil *et al.* (2010) with PNe and by Schuberth *et al.* (2010) with GCs. The phase-space plot for PNe around NGC 1399 in Fig. 1b shows three components, including PNe from NGC 1399 around $V_{1399} \simeq 1400$km/s, PNe from the lower-luminosity ETG NGC 1404 close-by in projection, and finally PNe from a component of "low-velocity outliers" with velocities $\sim 750 \pm 250$km/s.

The non-equilibrium low-velocity component is also seen in both the blue and red globular clusters around NGC 1399. The number density profile of red GCs approximately follows stellar light in this galaxy, whereas that of blue GCs does not. The decontaminated system of red GCs appears to be in approximate dynamical equilibrium, but this seems not the case for the blue GCs (Schuberth *et al.* 2010). This could be related to the fact that blue GCs are particularly prominent in smaller galaxies (Strader *et al.* 2006) which would be preferentially accreted at late times.

Indications for substructure have been found also in the halos of M87 and NGC 4649 (Romanowsky *et al.* 2012; Coccato *et al.* 2012). A fraction of large ellipticals have a

second galaxy within a $10-20'$ field. With discrete tracers (PNe or GCs) it is possible to eliminate kinematic substructures, which is a prerequisite for a reliable dynamical mass determination in such systems.

4.4. *Dark halo circular velocity curves and densities from stellar kinematics*

Using absorption line kinematics to 1-2R_e for luminous round ETGs, and nonparametric spherical distribution function models in combined luminous and dark halo potentials, Gerhard *et al.* (2001) found that the CVCs of ETGs are approximately flat. A more recent analysis of a sample of ETGs in the Coma cluster with $M_B = [-18.8, -22.6]$ and kinematic data out to $1-3\,R_e$ with axisymmetric Schwarzschild models by Thomas *et al.* (2007) showed somewhat more varied CVC shapes. Massive ETGs tend to have flat CVCs (e.g., NGC 4649, Das *et al.* 2011), while lower-mass ETGs (see §4.5) are also consistent with slightly decreasing CVCs. These studies agree in their derived DM fractions, $\sim 10-40\%$ within R_e, assuming constant M/L for the stellar component, which is also consistent with models of inner 2D kinematics by Cappellari *et al.* (2006).

Both studies also agreed in finding significantly higher central dark matter densities in ETGs than in spiral galaxies of the same luminosity or mass. For the Coma ETGs, Thomas *et al.* (2009) found a factor of 7× higher mean DM density within $2R_e$ at the same stellar mass, and 13× at the same luminosity. Baryonic contraction is not sufficient to explain this difference. One simple explanation is that the cores of ETG halos assembled earlier (at redshifts 1-3) than spirals of same luminosity (Gerhard *et al.* 2001; Thomas *et al.* 2009). Good agreement of the dynamical luminous plus dark matter models was found with SLACS lensing models of Auger *et al.* (2009); see Thomas *et al.* (2011).

4.5. *Mass Distributions of Quasi-Keplerian Ellipticals*

Méndez *et al.* (2001) first showed that the steeply decreasing outer velocity dispersion profile of the intermediate-luminosity elliptical (ILE) galaxy NGC 4697 could be matched well with an isotropic Hernquist model. They thus concluded that no evidence for dark matter had been found out to $3R_e$, but that dark matter could be present if the velocity distribution is anisotropic. Romanowsky *et al.* (2003) drew attention to three further ILEs with steeply decreasing $\sigma_p(R)$, NGC 821, 3379, and 4494, suggesting the presence of little if any dark matter in their halos. However, the well-known mass-anisotropy degeneracy (Binney & Mamon 1982) is much stronger in galaxies such as these ILEs, with de Vaucouleurs type luminosity profiles and steeply decreasing σ_p-profiles, than in galaxies with either more shallow luminosity profiles or radially constant projected velocity dispersions (Gerhard 1993).

With NMAGIC particle models (see de Lorenzi *et al.* 2007) based on a variety of kinematic data, including several hundred PN line-of-sight velocities, de Lorenzi *et al.* (2008, for NGC 4697), de Lorenzi *et al.* (2009, for NGC 3379) and Morganti *et al.* (2013, for NGC 4494) determined the range of quasi-isothermal halo potentials consistent with the data for these galaxies. Fig. 1c shows the 70% confidence boundaries from the PN likelihood for NGC 3379 and 4697, and from a more comprehensive analysis for NGC 4494. While some spread in the allowed CVCs and anisotropies remains, as expected, dark matter is required in all 3 galaxies. Fig. 1c indicates that the most favoured CVCs may be slightly falling, as in the lower-mass systems in Wu *et al.* (2012). Relative to the outer CVCs, the baryonic centers of these galaxies are quite centrally concentrated, as could be expected in gas-rich mergers.

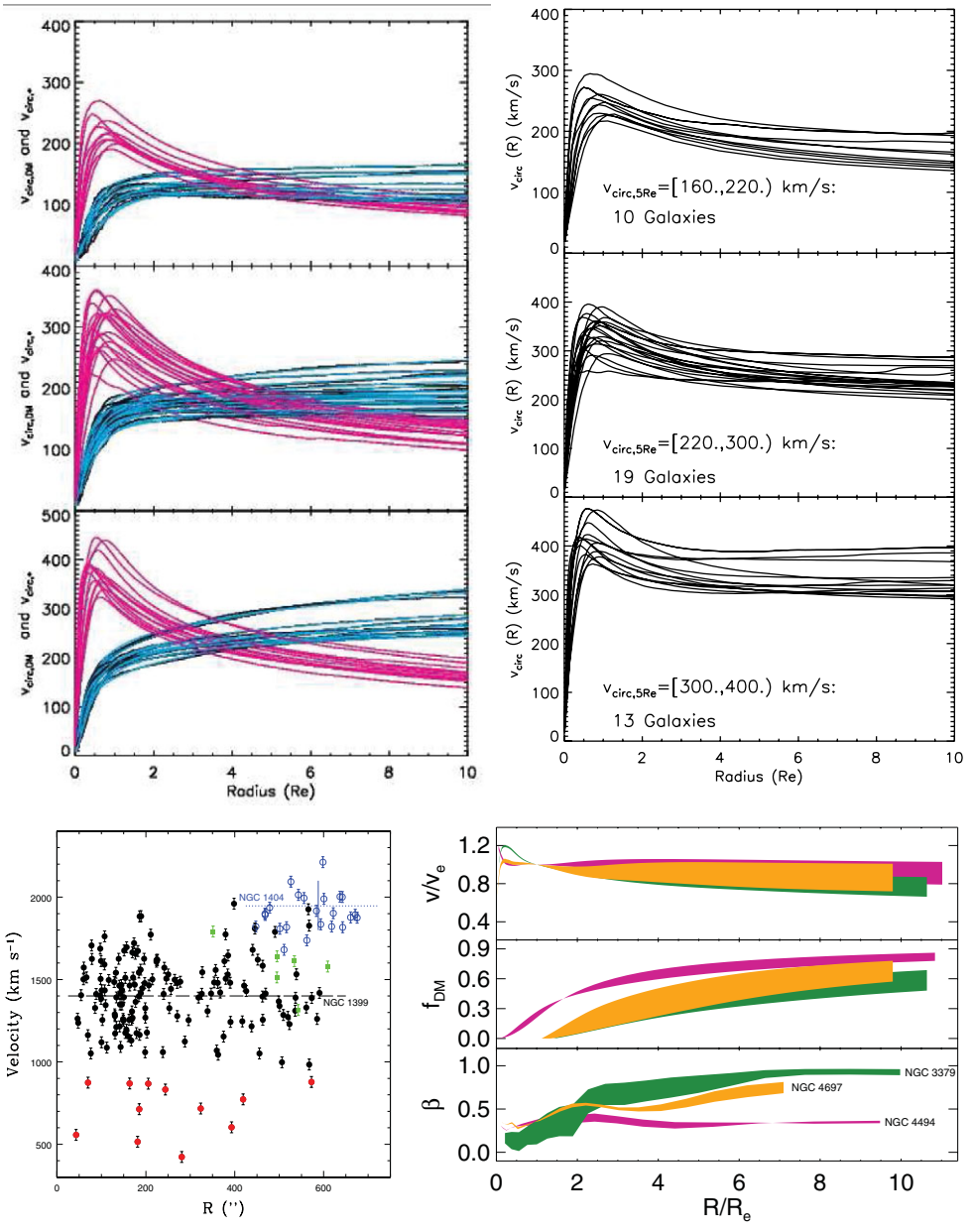

Figure 1. (a) Top: Circular velocity curves from stars (magenta), dark matter (black-blue, both left panel) and total mass distribution (right), for 42 model galaxies from the cosmological simulation of Oser *et al.* (2012), in bins of increasing total circular velocity at $5R_e$, as given on the right panels. From Wu *et al.* (2012). (b) Bottom left: Phase-space distribution of PNe in the nearby BCG galaxy NGC 1399 (black), its neighbour galaxy NGC 1404 (blue), and the low-velocity component (red). From McNeil *et al.* (2010). (c) Bottom right: 70% confidence ranges from dynamical modeling for total circular velocity normalized to value at R_e, DM fraction, and anisotropy parameter, for the three quasi-Keplerian ETGs NGC 3379, 4494, 4697. From Morganti *et al.* (2013).

4.6. *Dark Matter Fraction with Mass*

For radially constant mass-to-light ratio Υ, maximizing the fraction of mass following the luminosity profile results in a lower limit for the DM fraction, $f_{\rm DM,min}$. Dynamical modeling (§4.4, 4.5) gives $f_{\rm DM,min}(R < 1R_e) \simeq 0.1$-$0.4$ and $f_{\rm DM,min}(R < 5R_e) \simeq 0.3$-$0.8$, with a tendency of larger values for more massive ETGs. The corresponding $\Upsilon_{\rm max}$ also increase with galaxy mass (see Thomas *et al.* 2011). Napolitano *et al.* (2005) estimated gradients of Υ for a sample of ETGs with available dynamical mass modeling and found a correlation between luminosity and Υ-gradient such that the more luminous galaxies were more dark matter dominated. Comparing with DM halo predictions, the underlying reason appeared to be that the stellar bodies of brighter galaxies enclose a larger fraction of their DM halos. Deason *et al.* (2012) used power-law models to estimate dynamical masses at $5R_e$ for a sample of ETGs with extended PN and GC tracer kinematics. From their models they also found an increase of DM fraction inside $5R_e$ with galaxy mass, independent of whether a Chabrier or Salpeter IMF was assumed. The strong lensing results (§3.2) show a similar trend for the DM fraction within R_E.

Because dynamical $\Upsilon_{\rm max}$ increase with galaxy mass faster than stellar population Υ for given IMF, either some of the dark matter in massive ETGs must follow the light distribution, or the IMF must vary systematically with galaxy mass (Thomas *et al.* 2011). The latter interpretation is favoured by the dynamical analysis of Cappellari *et al.* (2012), and by new stellar population modeling of ETG spectra with NIR spectral features sensitive to low mass stars (Conroy & van Dokkum 2012). If the IMF varies between galaxies, it is natural in a hierarchical assembly picture to expect that it would also vary with radius within a galaxy. Reliable mass decomposition in ETGs will then require radially resolved spectral measurements of the IMF.

5. Conclusions

- Pure N-body simulations in ΛCDM cosmology predict nearly universal, prolate-triaxial DM halos. Including baryons and galaxy formation modifies the DM halo shapes, alignment, and inner density profiles. This provides one way to constrain the formation processes of the baryonic components.
- Weak lensing measurements are consistent with the predicted density structure of halos on large scales, and determine the relation between halo mass and galaxy luminosity.
- Mass determinations from strong lensing, X-ray emitting gas, stellar kinematics and PN kinematics out to several R_e find flat, close to isothermal CVCs for massive ETGs, while for lower mass, "quasi-Keplerian" ETGs the CVCs may be slightly falling.
- DM fractions at $5R_e$ inferred from dynamical modeling are in the range $\sim$ 30-80%. Inner DM densities in ellipticals are ~ 10 times higher than in spiral galaxies of the same stellar mass.
- A suite of recent high-resolution cosmological simulations of massive galaxies grown by minor and major mergers show systematic variations of the CVCs and DM fractions inside $5R_e$ with mass and fitted Sersic index, similar to those observed in ETGs.

References

Abadi, M. G., *et al.* 2010, *MNRAS*, 407, 435
Allgood, B., *et al.* 2006, *MNRAS*, 367, 1781
Arnaboldi, M., *et al.* 1996, *ApJ*, 472, 145
—. 1998, *ApJ*, 507, 759
Auger, M. W., *et al.* 2009, *ApJ*, 705, 1099

—. 2010, *ApJ*, 724, 511
Bailin, J. & Steinmetz, M. 2005, *ApJ*, 627, 647
Bailin, J., *et al.* 2005, *ApJ*, 627, L17
Barnabè, M., *et al.* 2009, *MNRAS*, 399, 21
—. 2011, *MNRAS*, 415, 2215
Berentzen, I. & Shlosman, I. 2006, *ApJ*, 648, 807
Bett, P., *et al.* 2010, *MNRAS*, 404, 1137
Binney, J. & Mamon, G. A. 1982, *MNRAS*, 200, 361
Blumenthal, G. R., Faber, S. M., Flores, R., & Primack, J. R. 1986, *ApJ*, 301, 27
Bolton, A. S., *et al.* 2008, *ApJ*, 682, 964
Brainerd, T. G., Blandford, R. D., & Smail, I. 1996, *ApJ*, 466, 623
Bullock, J. S., *et al.* 2001, *MNRAS*, 321, 559
Buote, D. A. & Humphrey, P. J. 2012, in Astrophysics and Space Science Library, Vol. 378, Astrophysics and Space Science Library, ed. D.-W. Kim & S. Pellegrini, 235
Cappellari, M., *et al.* 2006, *MNRAS*, 366, 1126
—. 2012, *Nature*, 484, 485
Churazov, E., *et al.* 2008, *MNRAS*, 388, 1062
—. 2010, *MNRAS*, 359
Ciotti, L. & Pellegrini, S. 2004, *MNRAS*, 350, 609
Coccato, L., Gerhard, O., & Arnaboldi, M. 2012, *MNRAS*, submitted (arXiv:1209.0356)
Coccato, L., *et al.* 2009, *MNRAS*, 394, 1249
Conroy, C. & van Dokkum, P. G. 2012, *ApJ*, 760, 71
Côté, P., *et al.* 2001, *ApJ*, 559, 828
Das, P., Gerhard, O., Churazov, E., & Zhuravleva, I. 2010, *MNRAS*, 409, 1362
Das, P., *et al.* 2011, *MNRAS*, 415, 1244
de Lorenzi, F., Debattista, V. P., Gerhard, O., & Sambhus, N. 2007, *MNRAS*, 376, 71
de Lorenzi, F., *et al.* 2008, *MNRAS*, 385, 1729
—. 2009, *MNRAS*, 395, 76
Deason, A. J., Belokurov, V., Evans, N. W., & McCarthy, I. G. 2012, *ApJ*, 748, 2
Deason, A. J., *et al.* 2011, *MNRAS*, 415, 2607
Diehl, S. & Statler, T. S. 2007, *ApJ*, 668, 150
Diemand, J. & Moore, B. 2011, Advanced Science Letters, 4, 297
Diemand, J., Moore, B., & Stadel, J. 2004, *MNRAS*, 353, 624
Diemand, J., *et al.* 2008, *Nature*, 454, 735
Doherty, M., *et al.* 2009, *A&A*, 502, 771
Douglas, N. G., *et al.* 2007, *ApJ*, 664, 257
Dubinski, J. & Carlberg, R. G. 1991, *ApJ*, 378, 496
Emsellem, E., *et al.* 2007, *MNRAS*, 379, 401
Ferreras, I., Saha, P., & Williams, L. L. R. 2005, *ApJ*, 623, L5
Fischer, P., *et al.* 2000, *AJ*, 120, 1198
Foster, C., *et al.* 2011, *MNRAS*, 415, 3393
Gao, L., *et al.* 2004, *MNRAS*, 355, 819
Gavazzi, R., *et al.* 2007, *ApJ*, 667, 176
Gerhard, O., Kronawitter, A., Saglia, R. P., & Bender, R. 2001, *AJ*, 121, 1936
Gerhard, O. E. 1993, *MNRAS*, 265, 213
Gnedin, O. Y., Kravtsov, A. V., Klypin, A. A., & Nagai, D. 2004, *ApJ*, 616, 16
Gnedin, O. Y. & Zhao, H. 2002, *MNRAS*, 333, 299
Governato, F., *et al.* 2010, *Nature*, 463, 203
Grillo, C. 2012, *ApJ*, 747, L15
Hahn, O., Teyssier, R., & Carollo, C. M. 2010, *MNRAS*, 405, 274
Hayashi, E., Navarro, J. F., & Springel, V. 2007, *MNRAS*, 377, 50
Hoekstra, H., Yee, H. K. C., & Gladders, M. D. 2004, *ApJ*, 606, 67
Hoekstra, H., *et al.* 2005, *ApJ*, 635, 73
Hui, X., Ford, H. C., Freeman, K. C., & Dopita, M. A. 1995, *ApJ*, 449, 592

Humphrey, P. J., Buote, D. A., O'Sullivan, E., & Ponman, T. J. 2012, *ApJ*, 755, 166
Humphrey, P. J., *et al.* 2006, *ApJ*, 646, 899
Hwang, H. S., *et al.* 2008, *ApJ*, 674, 869
Jing, Y. P. & Suto, Y. 2002, *ApJ*, 574, 538
Kazantzidis, S., *et al.* 2004, *ApJ*, 611, L73
Klypin, A., Kravtsov, A. V., Valenzuela, O., & Prada, F. 1999, *ApJ*, 522, 82
Koopmans, L. V. E., *et al.* 2006, *ApJ*, 649, 599
Kronawitter, A., Saglia, R. P., Gerhard, O., & Bender, R. 2000, *A&AS*, 144, 53
Leier, D., Ferreras, I., Saha, P., & Falco, E. E. 2011, *ApJ*, 740, 97
Macciò, A. V., Dutton, A. A., & van den Bosch, F. C. 2008, *MNRAS*, 391, 1940
Macciò, A. V., *et al.* 2012, *ApJ*, 744, L9
Mandelbaum, R., *et al.* 2006a, *MNRAS*, 370, 1008
—. 2006b, *MNRAS*, 368, 715
Mashchenko, S., Wadsley, J., & Couchman, H. M. P. 2008, *Science*, 319, 174
McNeil, E. K., *et al.* 2010, *A&A*, 518, A44
McNeil-Moylan, E. K., Freeman, K. C., Arnaboldi, M., & Gerhard, O. E. 2012, *A&A*, 539, A11
Méndez, R. H., *et al.* 2001, *ApJ*, 563, 135
Moore, B., *et al.* 1998, *ApJ*, 499, L5
Morganti, L., *et al.* 2013, in preparation.
Murphy, J. D., Gebhardt, K., & Adams, J. J. 2011, *ApJ*, 729, 129
Nagino, R. & Matsushita, K. 2009, *A&A*, 501, 157
Napolitano, N. R., *et al.* 2005, *MNRAS*, 357, 691
—. 2009, *MNRAS*, 393, 329
—. 2011, *MNRAS*, 411, 2035
Navarro, J. F., Frenk, C. S., & White, S. D. M. 1996, *ApJ*, 462, 563
Navarro, J. F., *et al.* 2010, *MNRAS*, 402, 21
Oser, L., Naab, T., Ostriker, J. P., & Johansson, P. H. 2012, *ApJ*, 744, 63
Oser, L., *et al.* 2010, *ApJ*, 725, 2312
Parker, L. C., *et al.* 2007, *ApJ*, 669, 21
Peng, E. W., Ford, H. C., & Freeman, K. C. 2004, *ApJ*, 602, 685
Proctor, R. N., *et al.* 2009, *MNRAS*, 398, 91
Revnivtsev, M., *et al.* 2008, *A&A*, 490, 37
Romanowsky, A. J., *et al.* 2003, *Science*, 301, 1696
—. 2012, *ApJ*, 748, 29
Rusin, D. & Kochanek, C. S. 2005, *ApJ*, 623, 666
Schuberth, Y., *et al.* 2010, *A&A*, 513, A52
Sellwood, J. A. & McGaugh, S. S. 2005, *ApJ*, 634, 70
Springel, V., *et al.* 2008, *MNRAS*, 391, 1685
Strader, J., Brodie, J. P., Spitler, L., & Beasley, M. A. 2006, *AJ*, 132, 2333
Teodorescu, A. M., *et al.* 2005, *ApJ*, 635, 290
—. 2011, *ApJ*, 736, 65
Thomas, J., *et al.* 2007, *MNRAS*, 382, 657
—. 2009, *ApJ*, 691, 770
—. 2011, *MNRAS*, 415, 545
Treu, T. 2010, *ARA&A*, 48, 87
Treu, T. & Koopmans, L. V. E. 2004, *ApJ*, 611, 739
Treu, T., *et al.* 2010, *ApJ*, 709, 1195
Trinchieri, G., *et al.* 2008, *ApJ*, 688, 1000
van Uitert, E., *et al.* 2011, *A&A*, 534, A14
—. 2012, *A&A*, 545, 71
Weijmans, A., *et al.* 2009, *MNRAS*, 398, 561
Woodley, K. A., *et al.* 2010, *AJ*, 139, 1871
Wu, X., *et al.* 2012, *MNRAS*, submitted (arXiv:1209.3741)